A heteroclinc surface between two saddle slow manifolds organizing sectors of rotation of mixed-mode oscillations

Elle Musoke, Bernd Krauskopf and Hinke M. Osinga
Department of Mathematics, The University of Auckland, Private Bag 92019, Auckland 1142, New Zealand

June 2023

Abstract

We investigate the mechanism underlying the generation of mixed-mode oscillations (MMOs) in the four-dimensional Olsen model for peroxidase-oxidase reaction. MMOs are characterized by a pattern of small-amplitude oscillations (SAOs) and large-amplitude oscillations (LAOs), and they are known to occur in systems with multiple timescales. We identify many co-existing MMO periodic orbits for the Olsen model. We show that these MMOs come in pairs and exist over a sequence of staggered ranges of the timescale separation parameter. In the four-dimensional phase space of the Olsen model, we find that the SAOs come about due to the geometry of a surface of heteroclinic connections between two saddle slow manifolds. We compute the surface of heteroclinic connections through a region of phase space that exhibits a slow passage through a Hopf bifurcation, where the SAOs are generated. Moreover, we compute its intersection curves with two well-chosen hyperplanes. In this way, we show how the surface of heteroclinic connections delimits rotational sectors with given numbers of subsequent SAOs, and also determines the exit from this region of SAOs and the onset of LAOs.

1 Introduction

Mixed-mode oscillations (MMOs) are characterized by their unique pattern of localized, small-amplitude oscillations (SAOs) followed by global, large amplitude oscillations (LAOs). MMOs are ubiquitous across many fields of application and appear, for example, in models for neuronal bursting [14, 23], lasers [19, 15], and chemical reactions [16, 2]. Systems that exhibit MMOs often feature multiple timescales, meaning that there is a difference in timescales along which system variables evolve. Studies of underlying mechanisms for generating MMOs have focused mainly on three-dimensional systems. A comprehensive review of such mechanisms in systems with multiple timescales, chiefly in phase spaces of dimension up to three, is presented in [4]; this survey also has a detailed list of references that covers the scope of where MMOs can be found in applications.

In its simplest form, there is a single timescale separation, given by a (small) parameter $\varepsilon > 0$, that divides the system into two groups of variables; such a system is also called a slow-fast system. It is part of a class of systems that can be analyzed with the tools of (standard) geometric singular perturbation theory (GSPT), as introduced in [9]; see also [17, 4]. The main result of GSPT is that in the limit $\varepsilon = 0$ one can derive lower-dimensional slow and fast subsystems from the original system, and their analysis gives insight into the dynamics of the full system. In particular, invariant objects of the two subsystems combine to form templates of observed slow-fast phenomena, such as spiking, bursting and MMOs. A key object in this regard is the critical manifold, which consists of branches or surfaces of equilibria of the fast subsystem that are separated by points or curves of bifurcation (where the stability of the equilibria changes). Away from these bifurcations, the critical manifold perturbs to slow

manifolds, which have the same dimension and stability properties, and along which the flow evolves on the slow timescale.

The geometry of the critical manifolds of the fast subsystem may create conditions that result in the existence of MMOs. Note that this requires a generator for SAOs as well as a global re-injection mechanism, associated with LAOs, back to the region of SAOs [4]. The possibilities for generating MMOs are limited by the dimension of the system. Two-dimensional systems have fast subsystems of dimension one. Consequently, the critical manifold is one dimensional with branches of attracting and repelling equilibria separated from each other by saddle node bifurcations (which are fold points with respect to the slow variable). Examples are the Van der Pol oscillator [30] and the FitzHugh–Nagumo equations [10, 23], which are well known for displaying two-timescale relaxation oscillations. The transition from small oscillations born in a Hopf bifurcation to large-amplitude relaxation oscillations famously involves what are know as canard orbits, which are characterized by following an unstable slow manifold for a considerable amount of time [1]. MMOs, on the other hand, require more dimensions and the lowest case is that of three-dimensional slow-fast models, which have either one or two fast variables. In the first case, there are two slow variable and the critical manifold is a surface, which may be folded along curves of saddle-node bifurcations. In the full system, the associated two-dimensional slow manifolds may intersect transversely near what are known as folded singularities on such fold curves [28, 31]. The resulting trajectories follow an unstable slow manifold and are, hence, canard orbits. How many canard orbits exist depends on the properties of the folded singularity in question; in particular, the canard orbits associated with a folded node divide the attracting slow manifold into sectors of rotation corresponding to different numbers of SAOs [3, 5]. In combination with a return mechanism that generates LAOs, this constitutes a mechanism for the creation of MMOs; see also [4] as an entry point to extensive literature on this mechanism. The second possibility for a three-dimensional model is that there are two fast variables and, hence, the critical manifold is of dimension one. It consists of branches that are either attracting, repelling or of saddle type, which meet at saddle-node bifurcations (fold points). Since the fast subsystem is now of dimension two, it may feature points of Hopf bifurcation that generate periodic orbits of the fast subsystem. SAOs may then be generated when trajectories of the full system slowly pass a Hopf bifurcation point of the fast subsystem, a phenomenon also known as a tourbillon [4]. Again, in the presence of a return mechanisms that generates LAOs, a tourbillon may result in the existence of MMOs.

Mechanisms for MMOs in higher-dimensional systems remain largely unexplored. However, there has been recent interest in how MMOs may arise and are organized in four-dimensional slow-fast systems [7, 13, 22], and this is also the setting of the work presented here. The fact that the phase space is now of dimension four opens possibilities for a wider range of singular system dynamics. In particular, a four-dimensional system may have a fast subsystem of dimension three. In this case, the associated critical manifold is again of dimension one, that is, consists of curves or branches of equilibria of the fast subsystem of different stability that meet at points of saddle-node and Hopf bifurcations. This is the general setting we study here, and the new aspect is that there may now be branches of saddle equilibria of different type, meaning that they have different numbers of stable and unstable directions. In this situation, two saddle branches of the critical manifold may be connected by a one-parameter family of heteroclinic connections, which perturbs to a surface of connections between two saddle slow manifolds in the full system. It was shown in [22] that this situation arises in the Olsen model for peroxidase-oxidase reaction. This earlier work focused on how this surface, which we refer to as $\mathscr{H}$, can be found in several steps by defining and solving appropriately formulated boundary value problems; in [22], we also showed that $\mathscr{H}$ is part of a global return mechanism for a pair of MMO periodic orbits.

In this paper, we present a comprehensive geometric picture of the role of the surface $\mathscr{H}$ of heteroclinic connections for the overall organization of MMOs in the Olsen model. To this

Table 1: Values of the parameters of system (1) as in [20] so that A, X, and Y are fast and B is slow.

α	δ	ε	λ	κ	μ	ζ
0.0912	1.2121×10^{-5}	0.0037	18.5281	3.7963	0.9697	0.9847

end, we exend and follow $\mathscr{H}$ through the region of the tourbillon. Moreover, we determine its intersection curves with different hyperplanes near the Hopf bifurcation of the fast subsystem. This is achieved with a continuation approach that defines the respective objects via solution families of suitably defined boundary value problems. In this way, we clarify the difference in the LAO structure between the co-existing pair of MMOs, which exist on an isola that extends over a finite interval of the timescale-separation parameter ε. Moreover, we identify many more such pairs of MMOs that differ in the number of their SAOs; their respective isolas overlap in ε, which means that many MMOs co-exist for a given value of ε. We present these co-existing MMOs together with the surface $\mathscr{H}$ of heteroclinic connections, globally in phase space as well as locally near the Hopf bifurcation point. This shows that $\mathscr{H}$ plays the role of a canard in this four-dimensional system in the sense that it determines rotational sectors corresponding to given fixed numbers of SAOs of the MMOs of the Olsen model.

This paper is organized as follows. In section 2, we present the Olsen model and some necessary background on how to apply GSPT to determine its slow-fast structure in the limit of $\varepsilon = 0$. Here, we also introduce the stable MMO periodic orbit Γ and its sister orbit on the primary isola, as well as the surface $\mathscr{H}$ of heteroclinic connections. Section 3 then discusses the positions of Γ and its sister relative to $\mathscr{H}$. Section 4 presents a further nine isolas with a total of 18 MMO periodic orbits, all of which co-exist with Γ and its sister orbit. We then show in Section 5 how the SAOs of the co-existing MMOs are organized by rotational sectors. We conclude in Section 6 with a brief discussion. Appendix A briefly summarizes the setup from [22], of the boundary value problem that was used to compute the surface $\mathscr{H}$.

2 The Olsen model and its slow-fast structure

The Olsen model for peroxidase-oxidase reaction as studied here was first introduced in [25, 24]. This biochemical reaction involves many steps, for which Olsen identified a minimal reaction scheme involving two intermediate free radicals. The resulting mathematical model is four dimensional and exhibits bistability, chaos, and MMOs in different parameter regimes. As in [22], we consider the Olsen model in a scaled form as presented by [20] and given by equations

$$\begin{cases} \dfrac{dA}{dt} = \mu - \alpha A - ABY, \\ \dfrac{dB}{dt} = \varepsilon(1 - BX - ABY), \\ \dfrac{dX}{dt} = \lambda(BX - X^2 + 3ABY - \zeta X + \delta), \\ \dfrac{dY}{dt} = \kappa\lambda(X^2 - Y - ABY). \end{cases} \tag{1}$$

Here, $(A, B, X, Y) \in \mathbb{R}^4$ represent four chemical concentrations. System parameters, represented by Greek letters in equation (1), are chosen as in [20] and given in Table 1; for notational

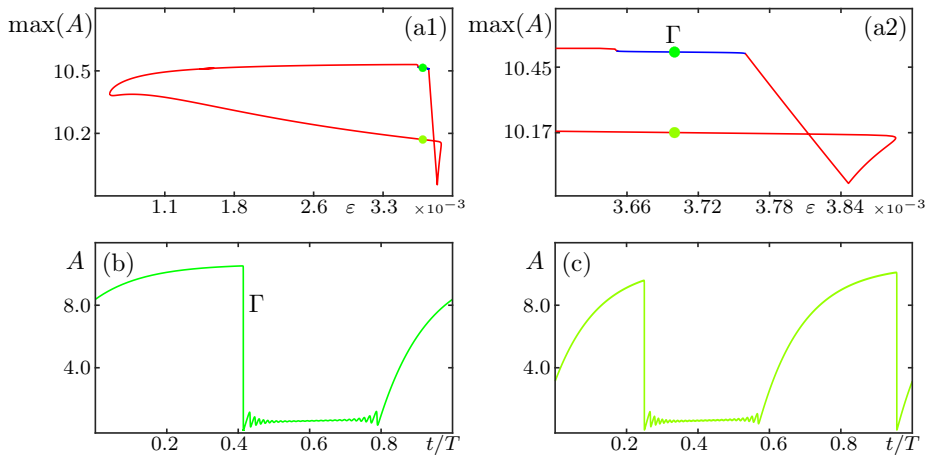

Figure 1: MMO periodic orbits of (1) forming an isola when continued in ε. Panel (a1) shows the entire isola, where the MMOs are represented by their maximum in A, and panel (a1) is an enlargement near the stable segment (blue); the dots mark the two MMOs for $\varepsilon = 0.0037$. The time profiles for A over one period of the stable MMO periodic orbit Γ (green curve) is shown in panel (a), and that of its saddle-type sister orbit (yellow-green curve) in panel (b).

convenience, we denote the parameters ε_b and ε^2 from [20] as ε and $\frac{1}{\lambda}$ instead. For this choice of parameters, A, X, and Y are fast and B is slow, and ε is the timescale parameter between these two groups of variables. Moreover, for the specific choice of $\varepsilon = 0.0037$ the Olsen model (1) has an attracting MMO periodic orbit, denoted Γ, which has a peculiar geometry. It was shown in [22] that, when Γ is continued in ε, this MMO periodic orbit traces out a closed curve — an isola — with an upper and a lower branch that meet at saddle-node bifurcations. Hence, Γ coexists with a sister MMO periodic orbit, which is of saddle type (with one unstable Floquet multiplier).

These earlier results from [22] form the starting point for the work presented here, and they are illustrated in Figure 1. Panel (a1) shows the isola of MMO periodic orbits that is obtained by continuing the stable MMO periodic orbit Γ in ε; this family of MMOs is represented by the maximum value of the A-coordinate along the periodic orbit. The isola covers an ε-interval that is bounded by saddle-node bifurcations of periodic orbits. Branches where MMOs have at least one unstable Floquet multiplier are indicated in red, showing that the MMOs are stable in a much smaller range along the blue part of the isola; this is illustrated further in the enlargement panel (a2). The stable MMO periodic orbit Γ and its sister saddle MMO periodic orbit for $\varepsilon = 0.0037$ are indicated by dots; they are shown as timeseries of the variable A over one period in panels (b) and (c) of Figure 1, respectively; here, time has been scaled to $[0, 1]$ and represents the fraction of the period T of the respective MMO periodic orbit. The timeseries bring out the mixed-mode nature of these oscillations. Notice from panel (b) that the stable periodic orbit Γ features a sequence of SAOs whose amplitude initially decreases, reaches a minimum and then increases again, followed by a LAO with a much larger amplitude, before the oscillation repeats. Its sister MMO periodic orbit in panel (c), on the other hand, features a similar sequence of SAOs, followed by two LAOs, which is why we refer to it as a 2-LAO MMO. We remark that the amplitude profile of the SAOs is typical for the tourbillon mechanism of slow transition through a Hopf bifurcation [4].

The question arises how the phase space is organized to give rise to the differences between these two co-existing MMOs. The timeseries in Figure 1(b) and (c) suggest that this has to do with the slow-fast nature of (1), which may be explained with the tools of GSPT. We now present briefly how GSPT is applied to the Olsen model; see also [9, 17] for background information.

By setting $\varepsilon = 0$ in system (1) one obtains the fast subsystem

$$\begin{cases} \dfrac{dA}{dt} = \mu - \alpha A - A\,B\,Y, \\ \dfrac{dX}{dt} = \lambda\,(B\,X - X^2 + 3A\,B\,Y - \zeta X + \delta), \\ \dfrac{dY}{dt} = \kappa\,\lambda\,(X^2 - Y - A\,B\,Y), \end{cases} \tag{2}$$

in which the coordinate B becomes a system parameter because $\frac{dB}{dt} = 0$. The critical manifold C in the full (A, B, X, Y)-space consists of the one-parameter family of equilibria of (2) with B as a parameter. The stability of an equilibrium $p \in C$ is given by the 3×3 Jacobian matrix of system (2). More specifically, when p is hyperbolic, it may have zero, one, two or three eigenvalues with negative real part. This means that its linear stable eigenspace $E^s(p)$ has dimension j with $j \in \{0, 1, 2, 3\}$ and, simultaneously, the linear unstable eigenspace $E^u(p)$ has the complemetary dimension three $3-j$. Hence, according to the Stable Manifold Theorem [26, 27] p has a stable manifold $W^s(p)$ and an unstable manifold $W^u(p)$, which have the same dimensions as, and are tangent to $E^s(p)$ and $E^u(p)$, respectively. The number of stable directions of p divides the critical manifold C into branches, denoted C^i, that are separated from each other by bifurcations of the fast system (2), at which $p \in C$ has at least one eigenvalue with zero real part. The B-parameterized families of $W^s(p)$ and of $W^u(p)$ for $p \in C^i$ form the stable and unstable manifolds of dimension i of the branch, which we denote $W^s(C^i)$ and $W^u(C^i)$; here, $i = j + 1$ since C is one dimensional.

For the values of the parameters in Table 1, the critical manifold C of (1) is a Z-shaped curve that has four branches, as is shown in Figure 2. The projection onto the (B, A)-plane in panel (a) shows the structure of C. Along the branch C^4_+, equilibra of (2) are stable. As B is increased, one encounters the saddle-node bifurcation point F_1 where C folds (very sharply) and turns into the saddle branch C^3. As B is then decreased, a second saddle-node bifurcation point F_2 is encountered, where C folds once again and turns into the saddle branch C^2. Immediately past F_2, points on C^2 have two real unstable eigenvalues. As B is increased, they become complex conjugate, and near $B \approx 0.9$ there is a Hopf bifurcation H of the fast subsystem. Past the point H, for increasing B, the equilibra of (2) are again stable along the branch C^4_-.

According to GSPT [9, 17], away from the bifurcation points F_1, F_2 and H the branches C^i of the critical manifold C perturb for small $\varepsilon > 0$ to slow manifolds S^i with the same stability properties. The dynamics on the S^i evolves on the slow timescale, as given by the slow subsystem, which is obtained by rescaling time to the slow time scale $\tau = \varepsilon t$ and again setting $\epsilon = 0$. For the Olsen model (1) this gives the differential algebraic system

$$\begin{cases} 0 &= \mu - \alpha A - ABY, \\ \frac{dB}{d\tau} &= 1 - BX - ABY, \\ 0 &= \lambda(BX - X^2 + 3ABY - \zeta X + \delta), \\ 0 &= \kappa\lambda(X^2 - Y - ABY). \end{cases} \tag{3}$$

Note that the critical manifold C is given by the algebraic part of system (3). The dynamics on C^i is given by $\frac{dB}{d\tau}$, which also determines the dynamics on the corresponding slow manifold S^i for small $\varepsilon > 0$. Moreover, the global manifolds $W^s(C^i)$ and $W^u(C^i)$ perturb to stable and unstable manifolds, denoted $W^s(S^i)$ and $W^u(S^i)$, respectively, of the slow manifolds S^i. For each branch C^i, the perturbed objects S^i, $W^s(S^i)$, and $W^u(S^i)$ are not unique. However, they lie exponentially close to each other. A method for computing a selected slow manifold S^i as a unique, isolated object is described in [22].

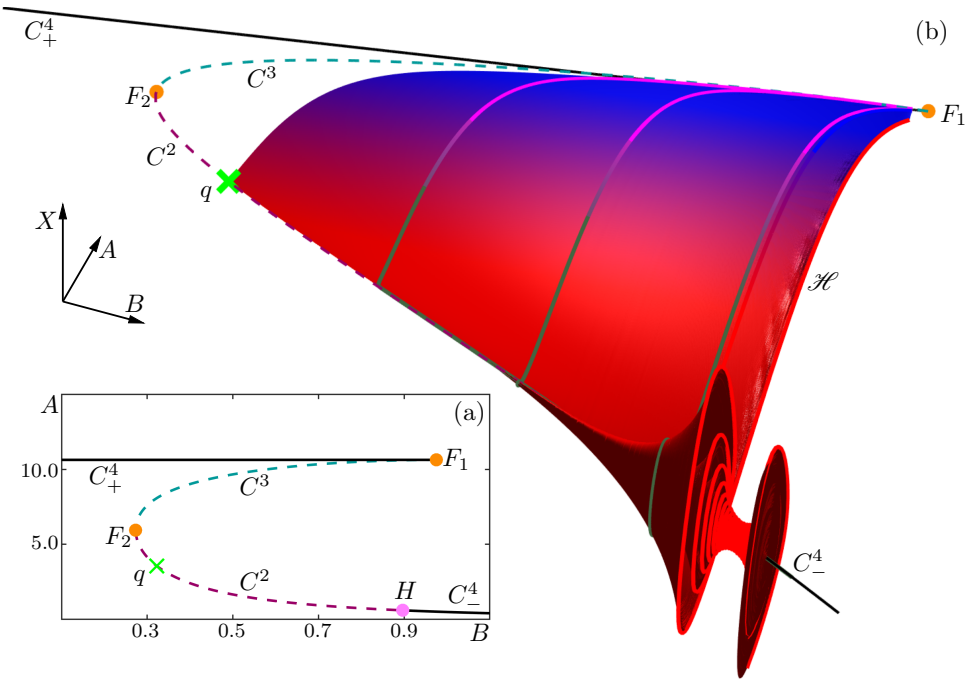

Figure 2: The critical manifold C is divided by the bifurcation points F_1, F_2 (orange dots) and H (pink dot) into the branches C^4_+ (solid black curve), C^3 (dashed teal curve), C^2 (dashed raspberry curve) and C^4_- (solid black curve), shown in projection onto the (B, A)-plane in panel (a) and onto (B, A, X)-space in panel (b); the point $q \in C^2$ (green cross) is an equilibrium of the full system. Panel (b) also shows the surface $\mathscr{H}$ of heteroclinic connections for $\varepsilon = 0.0037$ between the associated slow manifolds S^2 and S^3; the color changes from red near S^2 to blue near S^3, and highlighted are three individual connecting orbits on $\mathscr{H}$ (curves shaded forest green to magent).

Note from the discussion above that C^2 and C^3 and, hence, S^2 and S^3, have different dimensions of their global manifolds. Specifically, $W^u(S^2)$ and $W^s(S^3)$ are both three dimensional, and this means that they may robustly intersect in a two-dimensional surface in the four-dimensional phase space of (1). That this is indeed the case was shown in [22], where a numerical method based on what is know as Lin's method has been developed and implemented to find the slow manifolds S^2 and S^3 and the surface $\mathscr{H} = W^u(S^2) \cap W^s(S^3)$ of heteroclinic connecting orbits between them. The required setup for the boundary value problem is discussed in geometric terms in Appendix A; further implementation details can be found in [22].

Figure 2(b) shows the surface $\mathscr{H}$ of connecting orbits between the saddle slow manifolds S^2 and S^3 for $\varepsilon = 0.0037$, together with the branches of the critical manifold, in projection onto (B, A, X)-space. In this and subsequent three-dimensional renderings, we indicate the chosen viewpoint by including a coordinate frame that indicates the directions along which the variables increase. Shown on the surface $\mathscr{H}$ are three individual orbits from very near C^2 to very near C^3. They can be seen to oscillate slowly away from C^2 before crossing over to C_3, which they approach very slowly as B increases. The branch C^2 contains an equilibrium of the full system, denoted q, where the slow flow changes direction. The point q (or rather its two-dimensional unstable manifold; see [22]) marks the boundary of the surface $\mathscr{H}$. Observe that $\mathscr{H}$ starts to spiral around C^2 for higher values of B, where the eigenvalues of the equilibria are complex conjugate. Due to the slow drift along S^2 for $\varepsilon > 0$ the connecting orbits and, hence, the surface $\mathscr{H}$ itself can be computed past the Hopf bifurcation point H of the fast subsystem. Notice in Figure 2(b) how $\mathscr{H}$ takes the form of a scroll in this region with an amplitude envelope that decreases around C^2 and then increases around C^4_-.

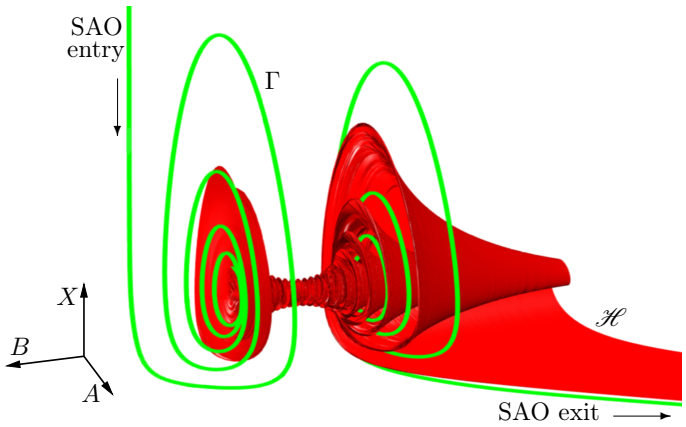

Figure 3: The SAO phase of the attracting MMO periodic orbit Γ during the transition through the tourbillon region is organized by the scrolling surface $\mathscr{H}$, shown in projection onto (B, A, X)-space.

3 The pair of MMO periodic orbits and the surface $\mathscr{H}$

The stable MMO Γ (as well as its sister periodic orbit) passes through the tourbillon region. This is shown in Figure 3 in an enlargement near the Hopf bifurcation point H, where the SAOs are generated; note that the viewpoint in Figure 3 is from a point with quite large A- and B-values, so that B is now decreasing to the right. The Hopf bifurcation point H of the fast subsystem is hidden by $\mathscr{H}$ and lies near where the amplitude of the scroll is minimal. Upon entry into the SAO region, Γ spirals in between the layers of the scrolling surface $\mathscr{H}$ as the amplitudes of its SAOs decrease before, and increase past the point H. This generates a given number of turns around the critical branches C^4_- and C^2, which translates to the same number of SAOs for Γ; compare with Figure 2(b). The stable MMO orbit Γ only exits the tourbillon region and completes its SAOs as soon as Γ spirals below $\mathscr{H}$; as can be seen in Figure 3, the MMO orbit Γ closely follows $\mathscr{H}$ as it crosses over to the branch C^3, which marks the beginning of its LAO.

Figure 3 suggests that the surface $\mathscr{H}$ of heteroclinic connections is involved in both the generation of SAOs, as well as their termination and the onset of the subsequent return mechanism. This motivates us to detemine in detail the geometry of $\mathscr{H}$ and how it relates to MMO periodic orbits. To this end, we compute the intersection set of $\mathscr{H}$ with suitably chosen three-dimensional sections that 'slice through' the tourbillon region. Specifically, we consider two sections through the point $H = (H_A, H_B, H_X, H_Y)$ of Hopf bifurcation of the fast subsystem. The section Λ_{H_B} of constant B given by

$$\Lambda_{H_B} := \{w = (w_A, w_B, w_X, w_Y) \in \mathbb{R}^4 \;\big|\; w_B = H_B\}$$

and the section

$$\mathscr{T} := \{w = (w_A, w_B, w_X, w_Y) \in \mathbb{R}^4 \;\big|\; w_X = \tfrac{1}{2}(w_A - H_A) + H_X\}, \tag{4}$$

which is perpendicular to Λ_{H_B} at H and contains the branches C^2 and C^4_- to good approximation.

We begin the discussion of the role of $\mathscr{H}$ by considering the 1-LAO periodic orbit Γ and its 2-LAO sister, where we focus on the exit from the tourbillon region and the beginning of the return mechanism that explains the difference between these two co-existing MMOs. Figure 4 shows Γ and its 2-LAO sister in projection onto (B, A, X)-space in panels (a) and (b), respectively, both together with the respective parts of the branches of the critical manifold from Figure 2(a). The

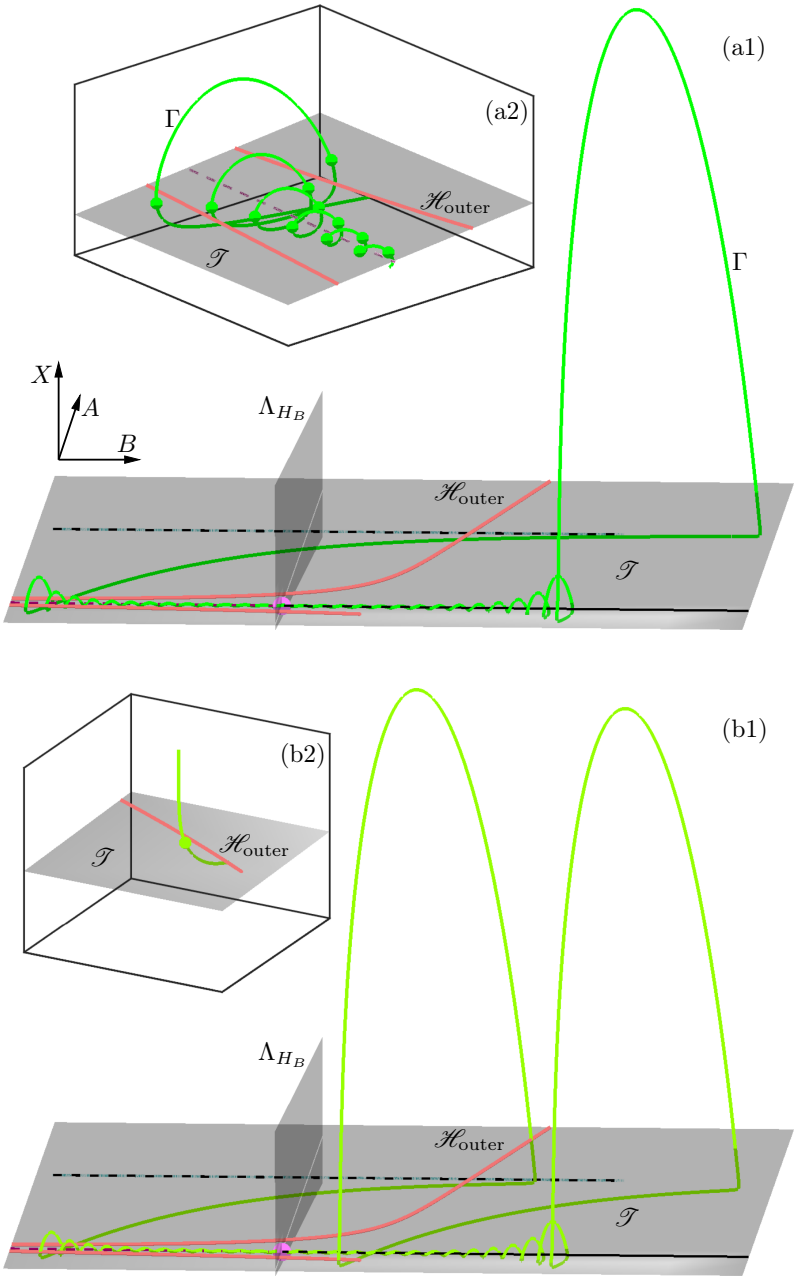

Figure 4: The attracting MMO Γ (green curve) and its 2-LAO sister (yellow-green curve) for $\varepsilon = 0.0037$, each shown in projection onto (B, A, X)-space in relation to the locus $\mathscr{H}_{\text{outer}}$ (coral curves) in the section $\mathscr{T}$ (charcoal plane), with a global view in panels (a1) and (b1), and as enlargements near $\mathscr{H}_{\text{outer}}$ in panels (a2) and (b2), respectively.

new elements in Figure 4 are the sections $\mathscr{T}$ and Λ_{H_B}, which appear as planes in this three-dimensional projection. Observe how Γ is entering the region of SAOs and 'weaves' through the section $\mathscr{T}$, generating two intersection points per turn, one on each side of the branches C^4_- and C^2. Indeed, the definition of $\mathscr{T}$ in (4) was chosen to have this property, as well as having an intersection with the fast LAO part of the MMO. The intersection $\mathscr{H} \cap \mathscr{T}$ is a collection of curves bounded by a pair of outermost intersection curves, which we refer to as $\mathscr{H}_{\text{outer}}$. These two curves are shown in Figure 4, and they determine the end of the SAO phase of the MMO.

Figure 4(a1) is a global view of the MMO periodic orbit Γ relative to $\mathscr{H}_{\text{outer}} \subset \mathscr{T}$ and

panel (a2) is an enlargement near the end of the SAO phase. At the end of its LAO, Γ enters the tourbillon region between the two curves of $\mathscr{H}_{\text{outer}}$. It then weaves through the section $\mathscr{T}$ to generate 28 SAOs while slowly moving to the left in the figure, remaining between the two curves of $\mathscr{H}_{\text{outer}}$. As the enlargement panel (a2) shows, the last SAO takes Γ to the outside of the two curves in Γ, and it then moves towards the branch C^3 as it closely follows the surface $\mathscr{H}$; see also Figures 3 and 2(b). The approach to C^3 is at an intermediate speed: only after following C^3 past the fold point F_1 does Γ enter into the last phase of its LAO, which consists of a large excursion in the fast variables X and Y that brings it back to the region of SAOs. Notice that this fast part of the orbit again intersects the section $\mathscr{T}$ in between the two curves of $\mathscr{H}_{\text{outer}}$ — or rather, to the right of the far curve in Figure 4(a1).

Figure 4(b1) shows in the same way a global view of the 2-LAO sister. Again we observe that this MMO enters the region of SAOs and then weaves through the section $\mathscr{T}$ in between the two curves of $\mathscr{H}_{\text{outer}}$. This periodic orbit completes only 27 SAOs before reaching the outside of $\mathscr{H}_{\text{outer}}$ and starting the transition back to the branch C^3 along the surface $\mathscr{H}$. However, before the fold point is reached, there is a very fast transition involving X and Y, which ends the first LAO. Notice that this part of the orbit intersects $\mathscr{T}$ to the left of the far curve of $\mathscr{H}_{\text{outer}}$. As is illustrated in the enlargement in Figure 4(b2), this implies that the orbit immediately starts another transition back to the branch C^3, without generating a SAO. This second transition takes the orbit past the fold point and the far curve of $\mathscr{H}_{\text{outer}}$, so that the second LAO brings the MMO periodic orbit back to the beginning of its SAO phase.

Figure 5 illustrates in more detail how $\mathscr{H}$ organizes the SAO regime. Shown in projection onto (B, A, X)-space in panels (a1) and (b1) is how Γ and its 2-LAO sister weave through $\mathscr{T}$ up to the section Λ_{H_B}. We show not only the locus $\mathscr{H}_{\text{outer}}$ but many more curves of the intersection set $\mathscr{H} \cap \mathscr{T}$, which form a ribcage-like structure. Also shown is the intersection set $\mathscr{H} \cap \Lambda_{H_B}$, which consists of a single curve in the form of a spiral. Note how the curves in $\mathscr{H}_{\text{outer}}$ intersect Λ_{H_B} indeed along the outermost part of the spiral. Notice also the part of the orbit in Figure 5(b1) that re-enters this region near Λ_{H_B} outside of the two curves in $\mathscr{H}_{\text{outer}}$. The enlargement panels (a2) and (b2) show a projection of the section $\mathscr{T}$ onto the (B, A)-plane near the re-entry of the respective MMO periodic orbit. Inside the region in $\mathscr{T}$ bounded by $\mathscr{H}_{\text{outer}}$, we see the SAOs of Γ and its 2-LAO sister weaving or lacing from region to region in between the rib-like curves in $\mathscr{H} \cap \mathscr{T}$ as they approach Λ_{H_B}. Comparing panels (a1) with (b1) and (a2) with (b2) shows that the consecutive intersection points of the two MMOs with $\mathscr{T}$ are separated by a sequence of ribs of $\mathscr{H} \cap \mathscr{T}$. The two intersection points in Figure 5(b2), which appear to lie on two curves in $\mathscr{H} \cap \mathscr{T}$, actually lie to the right of these curves.

Overall, we conclude from Figures 4 and 5 that, indeed, the surface $\mathscr{H}$ plays a major role in organizing the SAOs, as well as separating the SAOs from the LAOs, for the MMO Γ and its 2-LAO sister. In particular, the transition through the tourbillon is guided by the surface $\mathscr{H}$ in the sense that the respective part of the MMO orbit must 'spiral out' from the inside of the scroll to the outside before it can leave the SAO region. Notice from Figure 5 — by following the spiral $\mathscr{H} \cap \Lambda_{H_B}$ — that the rib-like curves in $\mathscr{H} \cap \mathscr{T}$ map to one another under the flow. In projection onto the (B, A)-plane these curves delineate regions that appear to play the role of sectors of rotation: the number of SAOs is determined by which region is entered at the end of the return mechnism given by the (last) LAO.

4 Additional isolas of MMOs

The apparent structure of sectors of rotation also suggests that other MMOs with different numbers of SAOs may well exist in the Olsen model. Indeed, it is well known that stable MMO periodic orbits may co-exist with several other saddle-type MMOs; see, for example, the case studies in [21, 29, 11, 12]. In this spirit, we found that the isola of Γ and its 2-LAO sister is

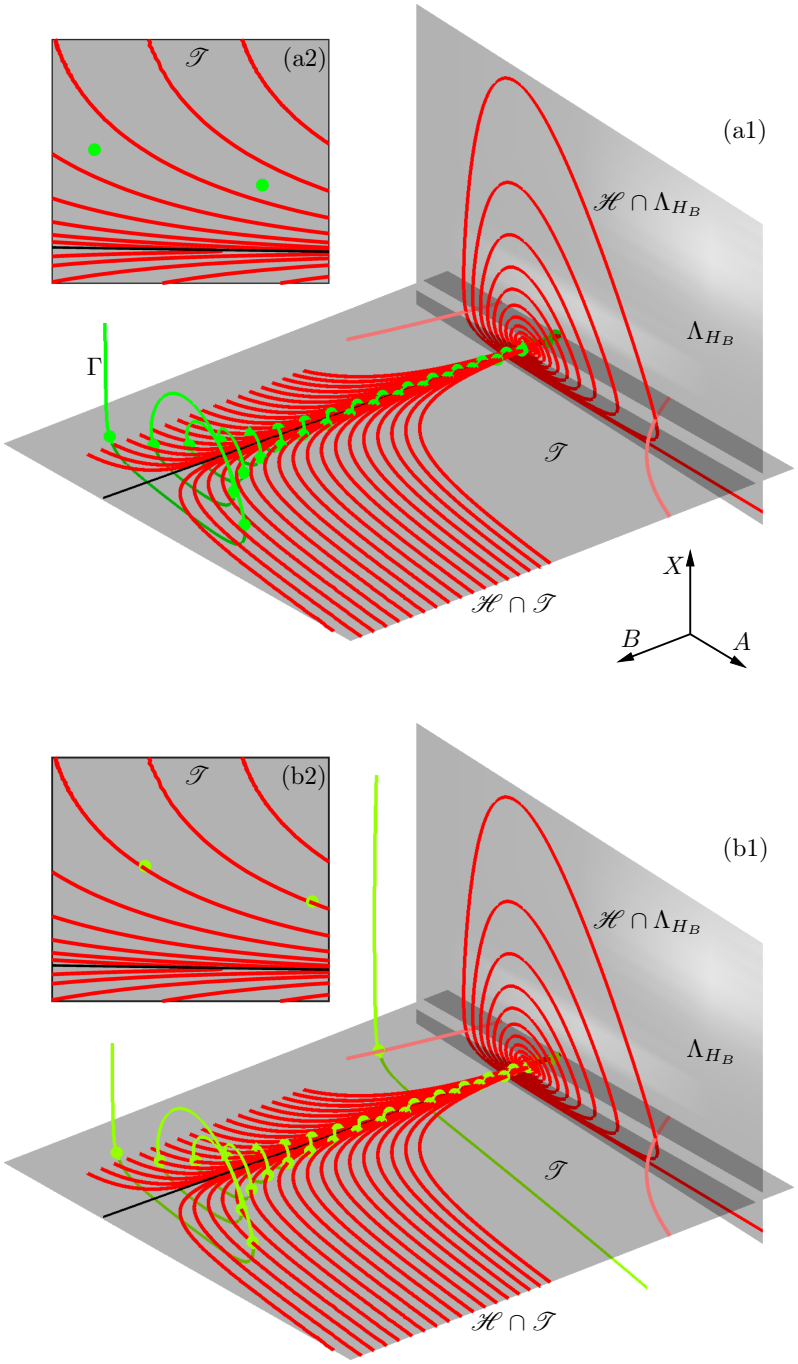

Figure 5: The stable MMO Γ (a1) and its 2-LAO sister (b1) in (B, A, X)-space with the loci $\mathscr{H} \cap \mathscr{T}$ and $\mathscr{H} \cap \Lambda_{H_B}$ (red curves) in the sections $\mathscr{T}$ and Λ_{H_B}, with enlargements in $\mathscr{T}$ (a2),(b2).

one of many isolas with other pairs of MMOs. Figure 6 shows ten of these isolas, where the MMO periodic orbits are again represented by the maximum of their A-values. The additional nine isolas were found by forward integration, searching for stable MMOs for different values of ε and then continuing them with respect to ε. Note that the isola from Figure 1(a1) is the top-most isola in Figure 6. Each isola covers a finite ε-interval and features a short segment where the respective 1-LAO periodic orbit is attracting and coexists with its saddle-type 2-LAO sister. Note that the stable segments on the isolas extend to increasingly larger values of ε, while their lengths increase to span a larger ε-interval; this is consistent with observations of isolas

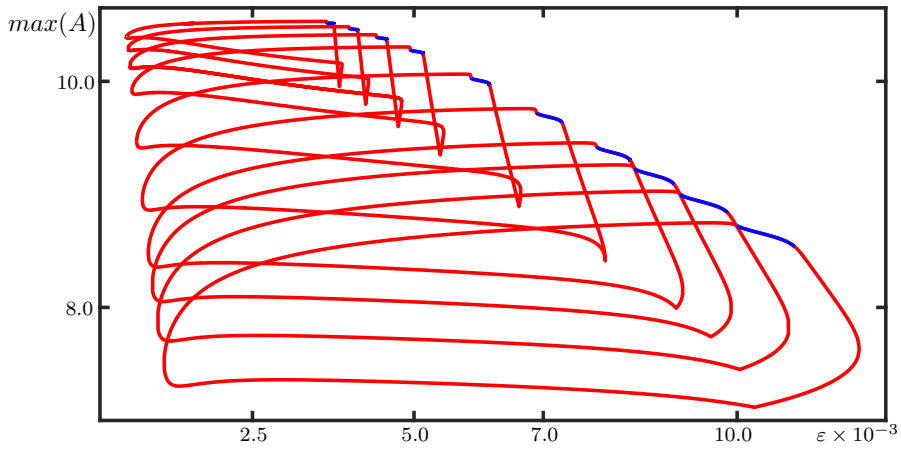

Figure 6: Isolas of MMO periodic orbits of (1) represented by the maximum of A versus ε; the respective MMO is stable along the blue segment and unstable otherwise. The top-most isola is the one from Figure 1(a1).

in [11, 13]. Note that the additional nine isolas all overlap with the stable region of the first, top-most isola in Figure 6. Hence, an additional 18 MMO periodic orbits exist for the value $\varepsilon = 0.0037$; with the exception of Γ, none of the computed MMOs are stable for this value of ε.

Figure 7 shows six co-existing MMO periodic orbits for $\varepsilon = 0.0037$, selected from the top three isolas in Figure 6 in relation to $\mathscr{H}_{\text{outer}} \subset \mathscr{T}$; the image shows the projection onto (B, A, X)-space. The presentation is as in Figure 4, and panels (a) of Figure 7 show Γ and the other two 1-LAO MMO periodic orbits from the upper branches of the three isolas, while panels (b) show their corresponding 2-LAO sisters, which lie on the lower branches of these three isolas. The 1-LAO MMOs in panel (a1) look very similar, but they differ in where they enter and exit the tourbillon region; see also the enlargement panel (a2). As a consequence, we find that the successive numbers of their SAOs differ by three. Similarly, the 2-LAO sister orbits in Figure 7(b1) look very similar, but they also differ in where they enter and exit the tourbillon region. Again we find that there is a change by three in the successive numbers of their SAOs. Notwithstanding this fact, the segments corresponding to the fast reinjection after their first LAOs lie much closer together. As panel (b2) illustrates, the points where these MMOs intersect the section $\mathscr{T}$ near the point H are very close together; note that these intersection points all lie beyond the lower curve of $\mathscr{H}_{\text{outer}}$, so that their second LAOs are triggered immediately.

5 Organization of SAOs and rotational sectors

We conclude that the difference from isola to isola is an overall change by three in their number of SAOs. This is illustrated further in Figure 8, where we show $\mathscr{T}$ in projection onto the (B, A)-plane near the entry to the SAO region, together with the curves in $\mathscr{H} \cap \mathscr{T}$ and the intersection points of the respective 1-LAO and 2-LAO periodic orbits from Figure 7; note that, as in Figure 7, the panels of Figure 8 are oriented in the direction of increasing B which means that they are rotated compared to Figure 5. In Figure 8, we labeled the regions in between the rib-like curves in $\mathscr{H} \cap \mathscr{T}$ by the number of observed SAOs that are generated by an initial condition in such a region. This confirms that the regions in the (B, A)-plane in between the curves of $\mathscr{H} \cap \mathscr{T}$ play the role of sectors of rotation: which region is entered after the last LAO determines the subsequent number of SAOs generated by the tourbillon mechanism, as the points 'hop' from sector to sector in this representation. Each 1-LAO MMO completes a number of SAOs that is one more than those of its 2-LAO sister MMO. Notice how the 1-LAO

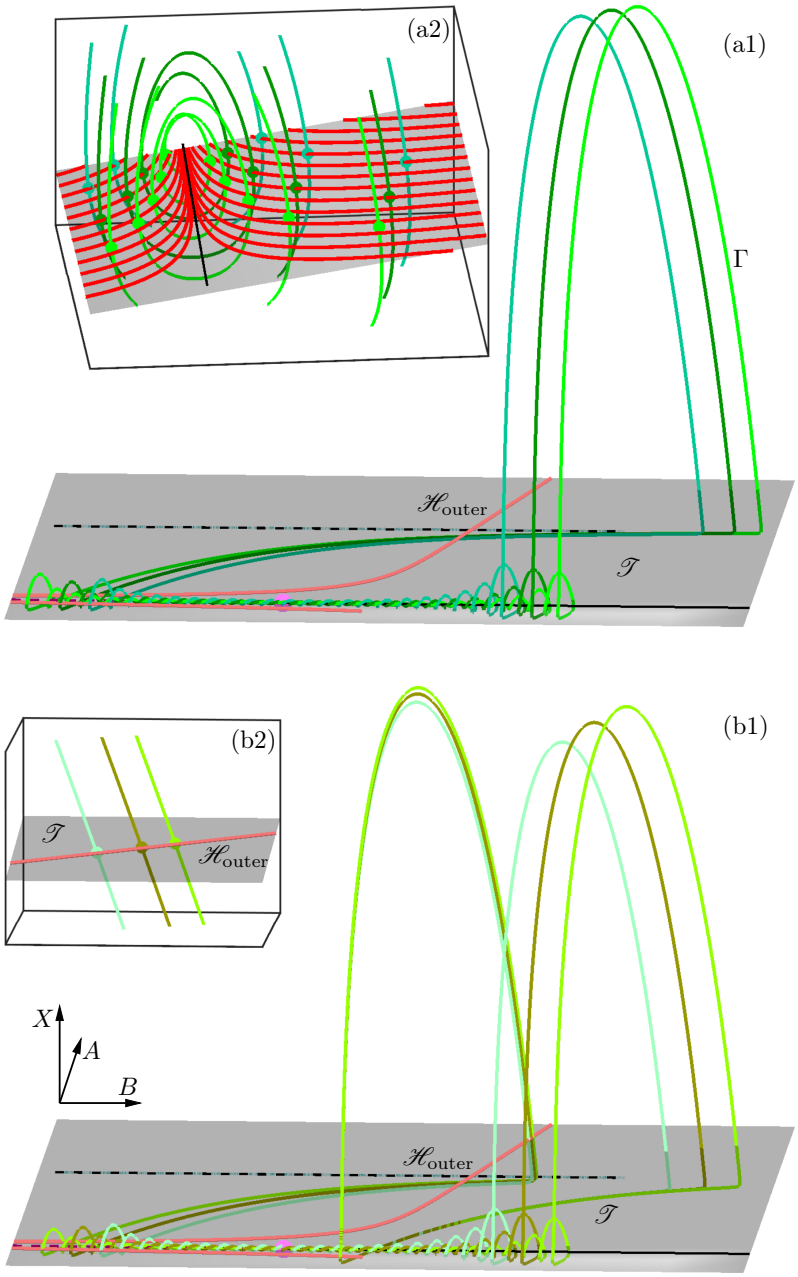

Figure 7: The 1-LAO MMOs and their 2-LAO sisters (various shades of green) for $\varepsilon = 0.0037$ from the top three isolas in Figure 6, each shown in projection onto (B, A, X)-space in relation to $\mathscr{H}_{\text{outer}} \subset \mathscr{T}$. Panels (a1) and (b1) show a global view, with panels (a2) and (b2) enlargements of the entry to the SAO phase with $\mathscr{H} \cap \mathscr{T}$, and the return to $\mathscr{T}$ after the first LAO, respectively.

MMOs of the two subsequent isolas intersects $\mathscr{T}$ in between two rib-like curves in $\mathscr{H} \cap \mathscr{T}$ that lie three, respectively six curves further to the left. Indeed, most of the intersection points are very close to curves in $\mathscr{H} \cap \mathscr{T}$, but closer inspection reveals that they do, in fact, lie to the left of these ribs.

These observations suggest that $\mathscr{H}$ plays a similar role in the organization of SAOs for the Olsen model as canard orbits formed by intersections of slow manifolds in systems with one fast and two slow variables; see [4, 31, 5]. More specifically, the theory for three-dimensional systems with two slow variables tells us that a two-dimensional, attracting slow manifold may be divided

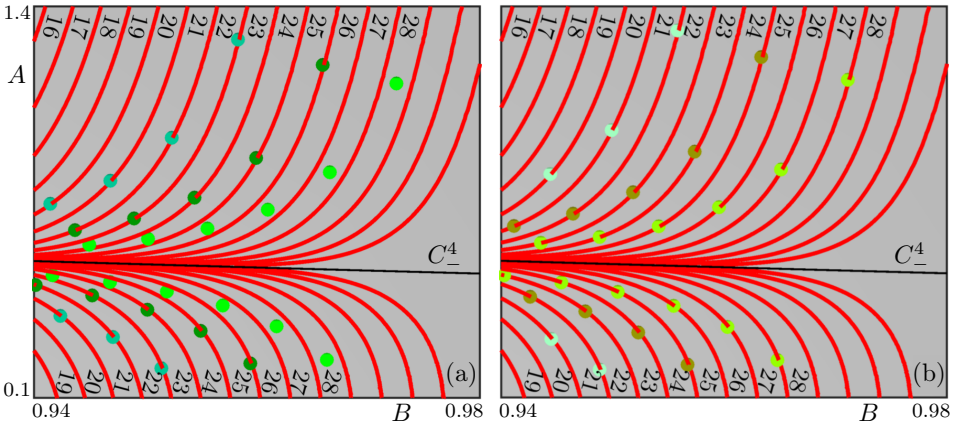

Figure 8: The 1-LAO MMOs in panel (a) and their 2-LAO sisters from Figure 6 in panel (b), shown in the (B, A)-plane at the beginning of the SAO phase as intersection points with the section $\mathscr{T}$ (dots of various shades of green) in relation to $\mathscr{H} \cap \mathscr{T}$ (red curves) and the (projected) branch C^4_- (black curve). The numbers respresent how many SAOs are to follow during the slow transition past the Hopf bifurcation.

into sectors of rotation that are separated from one another by one-dimensional canard orbits [4]. The number of SAOs that an MMO makes is then determined by the sector where the MMO enters the respective region of phase space, which is typically near a folded node of the system. A two-dimensional attracting slow manifold and canard orbits bounding rotational sectors on it can be computed as a one-parameter solution family of a boundary value problem [5, 6]. In [7], we explored a reduced, three-dimensional version of the Olsen model subject to a quasi steady-state assumption. We found that the stable manifold analogous to $W^s(S^3)$ is two dimensional and spirals around a branch analogous to C^2 of the critical manifold. Since an (orientable) two-dimensional manifold is a separatrix in three-dimensional space, the spiraling of the two-dimensional stable manifold is sufficient to generate and organize the SAOs for the MMOs in this reduced system. A similar observation was made in [8] for a three-dimensional system with one slow variable, where a two-dimensional stable manifold of a one-dimensional saddle slow manifold organizes the SAOs of so-called pseudo-plateau bursting orbits.

However, the Olsen model (1) has a four-dimensional phase space and the organization of its MMOs is not fully described by the reduced, three-dimensional Olsen model from [7]. Therefore, Figure 8 is somewhat misleading: even though the two-dimensional surface $\mathscr{H}$, when shown in projection onto (B, A, X)-space, appears to be similar in geometry to the analog of $W^s(S^3)$ in [7], it is not a separatrix in phase space. In particular, the intersection curves in $\mathscr{H} \cap \mathscr{T}$ are not separatrices in the three-dimensional section $\mathscr{T}$. Nevertheless, we are able to identify two-dimensional sectors of rotation in the projection onto the (B, A)-plane shown in Figure 8. To explain this paradox, we need to consider the timescale separation between the fast variable A and the fast variables X and Y. This is similar in spirit to the work in [13], where a two-dimensional slow manifold in a four-dimensional system is shown to play a role in determining rotational sectors. Figure 9 shows the critcal branch C^4_- and the intersection set $\mathscr{H} \cap \mathscr{T}$ together with the intersection points of Γ and its 2-LAO sister in the three-dimensional section $\mathscr{T}$, as represented by (B, A, Y)-space. Here, we also plot local segments of the curves Γ and its 2-LAO sister in projection onto (B, A, Y)-space. Note that these curve segments, which do not lie in $\mathscr{T}$ except for the intersection points shown, give an impression of the flow relative to the section. This representation illustrates that the intersection points of Γ and its 2-LAO sister lie at some distance from $\mathscr{H} \cap \mathscr{T}$. In other words, as is expected in a three-dimensional space, the curves in $\mathscr{H} \cap \mathscr{T}$ are not separatrices. Rather, the two-dimensional intersection set $W^s(S^3) \cap \mathscr{T}$ of

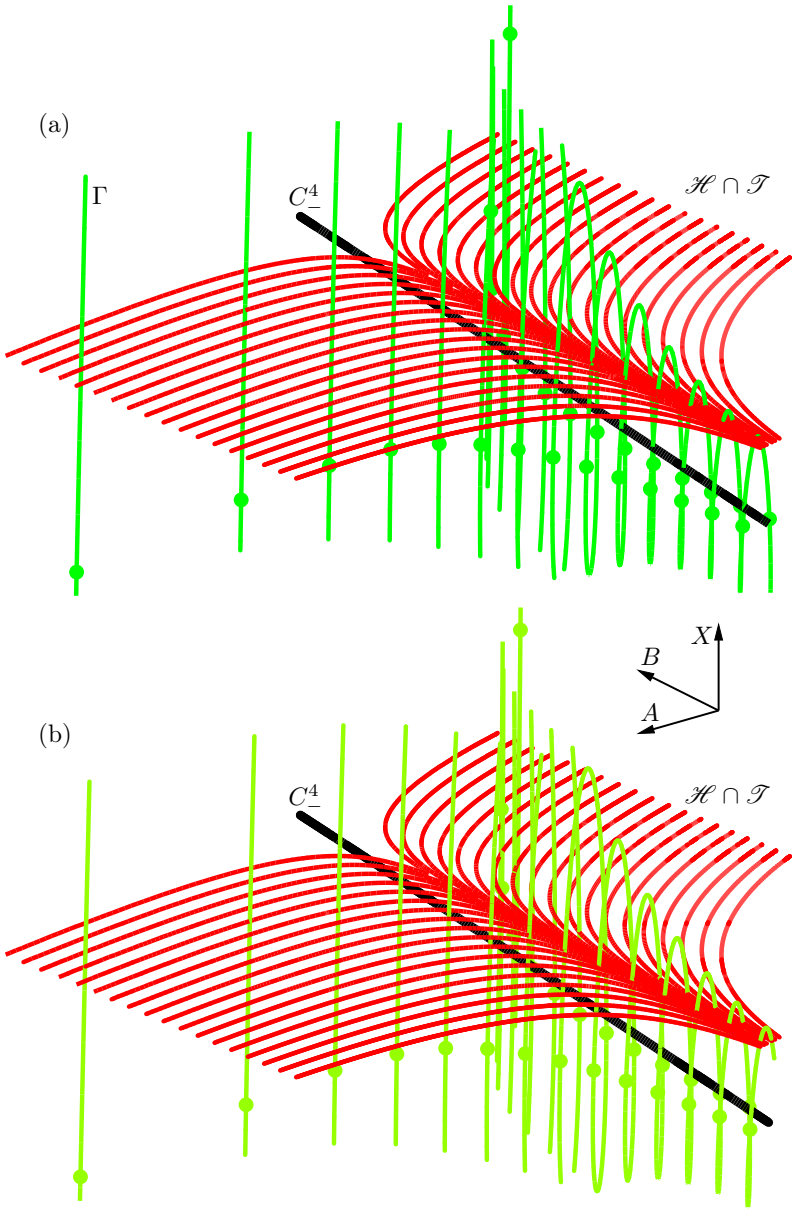

Figure 9: The intersection points (green dots) of the attracting MMO periodic orbit Γ (a) and its 2-LAO sister (b) at the beginning of the SAO phase, shown with $\mathscr{H} \cap \mathscr{T}$ (red curves) and C^4_- (black curve) in the three-dimensional (B, A, Y)-space representing the section $\mathscr{T}$. Also shown are the projections onto (B, A, Y)-space of local segments of the respective MMO periodic orbit (green curves).

the repelling slow manifold locally divides $\mathscr{T}$ into regions that correspond to different sectors of rotation on the attracting slow manifold $W^u(S^2) \cap \mathscr{T}$. Since $\mathscr{H} = W^s(S^3) \cap W^u(S^2)$, we have that $\mathscr{H} \cap \mathscr{T} \subset W^u(S^2) \cap \mathscr{T}$. The Y-direction in T, which is repelling, is actually three orders of magnitude faster than the repelling fast A-direction; this can be seen from the ratio $\frac{\alpha}{\kappa\lambda} \approx 1.2965 \times 10^{-3}$ of the respective linear parts in (1). Moreover, to very good approximation, the intersection set $\mathscr{H} \cap \mathscr{T}$ lies in a plane and the Y-direction is effectively perpendicular to this plane. Hence, for the local view of (B, A, Y)-space shown in Figure 9, the intersection set $W^s(S^3) \cap \mathscr{T}$ is a collection of effectively vertical walls that intersect the surface $W^u(S^2) \cap \mathscr{T}$ in the curves $\mathscr{H} \cap \mathscr{T}$. This means that the projection of $\mathscr{H} \cap \mathscr{T}$ along the Y-axis onto the

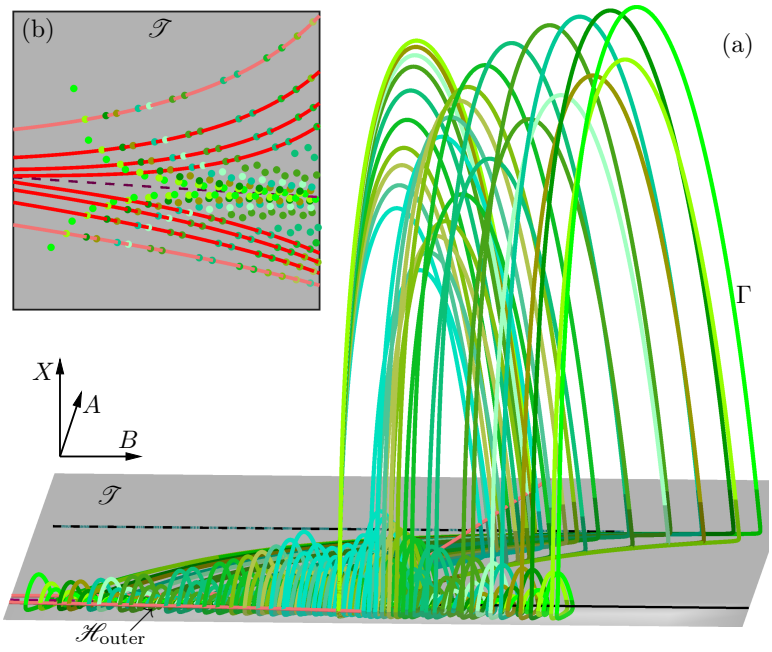

Figure 10: All coexising MMO periodic orbits (curves of various shades of green) for $\varepsilon = 0.0037$ on the isolas shown in Figure 6. Panel (a) is the projection onto (B, A, X)-space with $\mathscr{T}$ and $\mathscr{H}_{\text{outer}}$ (coral curve), and panel (b) is the projection onto the (B, A)-plane of the section $\mathscr{T}$ near the exit of the SAO phase with the corresponding intersection points (dots of various shades of green) relative to the four outermost intersection curves in $\mathscr{H} \cap \mathscr{T}$, which includes $\mathscr{H}_{\text{outer}}$ (coral curves).

(B, A)-plane, as in the bird's eye view in Figure 8, faithfully represents the three-dimensional rotational sectors: in fact, even though the intersection points with $\mathscr{T}$ in Figure 8 lie extremely close to some of the rib-like curves in $\mathscr{H} \cap \mathscr{T}$, their location in the (B, A)-plane relative to the curves in $\mathscr{H} \cap \mathscr{T}$ still determines the number of subsequent SAOs of a given trajectory. This was checked numerically for all of the MMOs for $\varepsilon = 0.0037$ on the ten isolas shown in Figure 6.

Figure 10 shows how these twenty MMO periodic orbits simultaneously weave through the section $\mathscr{T}$ as they drift through the tourbillon region. Panel (a) shows that their LAOs are ordered from right to left and have decreasing amplitudes as one moves down from isola to isola in Figure 6. The right-most LAO with the largest amplitude in Figure 10(a) is that of the attracting MMO Γ on the top-most isola, which has the most, namely, 28 SAOs; then follows, with a distinctly lower amplitude than that of the right-most LAO of Γ, the second LAO of its 2-LAO sister, which has 27 SAOs. Next is the 1-LAO MMO one isola down, which has 25 SAOs, followed by its 2-LAO sister, with 24 SAOs, and so on. Observe that the amplitudes of the LAOs for the 1-LAO periodic orbits, as well as both the first and second LAOs of their 2-LAO sisters decrease from one isola to the next; see also Figure 7. Note in Figure 10(a) that the ten 2-LAO MMOs return to $\mathscr{T}$ after their first LAOs at almost the same point near $\mathscr{H}_{\text{outer}}$, even though the amplitudes of these first LAOs before and of their second LAOs after the return to $\mathscr{T}$ differ significantly; we consider the precise mechanism that selects the amplitudes and relative locations of the LAOs beyond the scope of this paper.

Figure 10(b) shows the region past the point H of exit from the SAO region in $\mathscr{T}$ in projection onto the (B, A)-plane. We show only the four outermost pairs of curves of $\mathscr{H} \cap \mathscr{T}$ on either side of the branch C^2, including the two curves in $\mathscr{H}_{\text{outer}}$. As the MMO periodic orbits spiral towards lower values of B, their intersection points hop from region to region until they reach the outside of the two curves in $\mathscr{H}_{\text{outer}}$ and their SAO phase ends; compare with Figure 1(a2).

6 Conclusions

We studied the geometry of MMOs in the four-dimensional Olsen model for the peroxidase-oxidase reaction in a parameter regime where three variables are fast and one is slow. We found a large number of co-existing MMO periodic orbits that come in pairs of 1-LAO and 2-LAO MMOs on two branches that form isolas when continued in the timescale separation parameter ε. Their organization in the four-dimensional phase space and, in particular, how many SAOs they feature is determined by the geometry of the surface $\mathscr{H}$ of heteroclinic orbits between two saddle slow manifolds that have (un)stable manifolds of different dimensions. To show this, we computed and continued $\mathscr{H}$ through the SAO region near a Hopf bifurcation of the fast system. Moreover, we computed and presented the intersection set of this surface with a suitable three-dimensional section, which revealed sectors of rotation that organize the number of subsequent SAOs.

We conclude that the surface $\mathscr{H}$ of heteroclinic orbits between two saddle slow manifolds plays a characterizing and organizing role for the SAOs of the MMOs in the four-dimensional phase space. In particular, $\mathscr{H}$ divides the three-dimensional attracting slow manifold into sectors of rotation. While the tourbillon mechanism for SAOs in the Olsen model is different, the surface $\mathscr{H}$ nevertheless acts like the canard orbits near a folded node in a three-dimensional system, which divide the respective two-dimensional attracting slow manifold into sectors of rotation. When intersected with a transverse plane, this attracting slow manifold of the three-dimensional system is represented by a strongly attracting curve segment with rotational intervals bounded by the intersection points of the canard orbits. Similarly, in the three-dimensional section we considered for the Olsen model, $\mathscr{H}$ generates intersection curves that divide the strongly attracting intersection surface of the three-dimensional attracting slow manifold into sectors of rotation. We found that these sectors can faithfuly be represented in a two-dimensional plane, via the projection along a very fast variable, and they reliably predict the number of SAOs for all of the twenty compute MMO periodic orbits.

A Setup of the boundary value problem for $\mathscr{H}$

We used the method from [22] for locating and computing $\mathscr{H}$. For context, we describe the computational setup in a geometric way and refer to [22] for details of the mathematical formulation and implementation. It involves an unconventional implementation of Lin's method [18] in a four-dimensional phase space with the goal of finding a first orbit segment on $\mathscr{H}$. This is a non-trivial exercise because the surface $\mathscr{H}$ itself is a saddle object with a strongly attracting and a strongly repelling direction.

Figure 11 shows our setup in projection onto (B, A, X)-space of (1) with the two saddle branches C^3 and C^2 of the critical manifold and a three-dimensional section $\mathscr{L} = \{\omega \in \mathbb{R}^4 \mid \omega_A = 6.0\}$. This so-called Lin section, which appears as a plane in projection, contains the fold point F_2 and separates the branches C^3 and C^2. The task is to connect the slow manifold S^2, via the unstable manifold $W^u(S^2)$ and the stable manifold $W^s(S^3)$, with the slow manifold S^3. Specifically, we find an orbit segment $\mathbf{w}$ approximately on $W^u(S^2)$ with begin point in the linear unstable eigenspace $E^u(p_2)$ of a point $p_2 \in C^2$ close to the point H; its end point lies in the Lin section $\mathscr{L}$. Observe how $\mathbf{w}$ initially follows C^2 closely while drifing away from the point H and then quickly spirals out and finally reaches $\mathscr{L}$. Similarly, we find an orbit segment $\mathbf{u}$ approximately on $W^s(S^3)$ with begin point $\mathbf{u}(0) \in \mathscr{L}$ and end point $\mathbf{u}(1)$ in the linear stable eigenspace $E^s(p_3)$ of a point $p_3 \in C^3$ close to the fold point F_1. The orbit segment $\mathbf{u}$ moves quickly away from $\mathscr{L}$ and then approaches C^3, which it then follows closely.

Notice in Figure 11 how both $\mathbf{w}$ and $\mathbf{u}$ have a point of high curvature near the section $\mathscr{L}$, which they approach or leave, respectively, in an almost tangent fashion. This is due to the

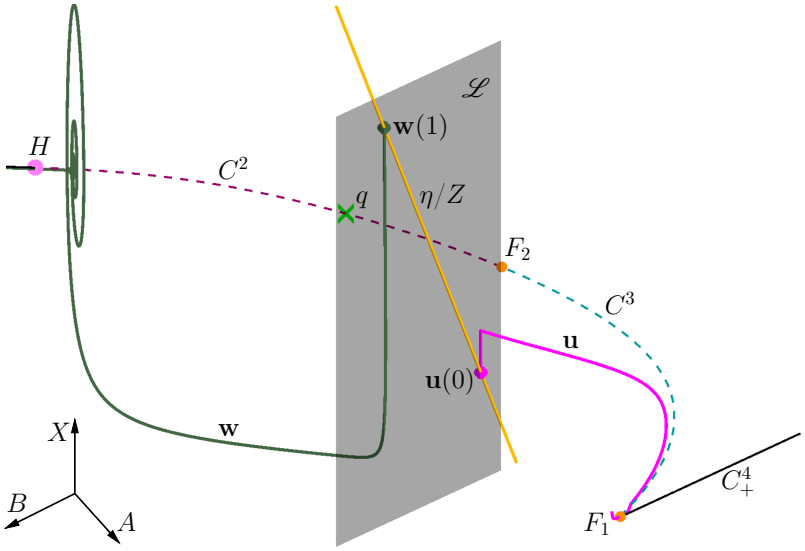

Figure 11: An intermediate step in the setup of Lin's method for computing the surface $\mathscr{H}$. Orbit segments $\mathbf{u} \in W^s(S^3)$ (magenta curve) and $\mathbf{w} \in W^u(S^2)$ (forest-green curve) begin and end in the Lin section $\mathscr{L}$ (charcoal plane), respectively. The begin point $\mathbf{u}(0)$ of $\mathbf{u}$ and the end point $\mathbf{w}(1)$ of $\mathbf{w}$ lie along the Lin space Z (gold line). Also shown are C^3, C^2, $C^4_\pm$, F_1, F_2, and q; compare with Figure 2.

strong contracting and expanding directions normal to the surface $\mathscr{H}$, and it highlights the extreme sensitivity of the Olsen model (1). This is why the orbit segments $\mathbf{w}$ and $\mathbf{u}$ cannot be obtained by shooting to the section $\mathscr{L}$. Rather, they are found by continuation as solution families of suitable boundary value problems, namely via two homotopy steps that increase the orbit first along the respective critical branch and then away from it until $\mathscr{L}$ is reached; see [22].

The key idea behind Lin's method as a computational tool is to couple the two orbit segments $\mathbf{w}$ and $\mathbf{u}$ by requiring that the points $\mathbf{u}(0)$ and $\mathbf{w}(1)$ inside $\mathscr{L}$ lie along the Lin space, denoted Z in Figure 11, which is one dimensional in our case; see [18] for more information. Crucially, the signed distance η between $\mathbf{u}(0)$ and $\mathbf{w}(1)$ along the fixed direction Z is a well-defined test function, whose zeros correspond to connecting orbits since then $\mathbf{w}(1) = \mathbf{u}(0)$. Continuation in η of $\mathbf{w}$ and $\mathbf{u}$, while Z is kept fixed but the respective position of $\mathbf{w}(0) \in E^u(p_2)$ and of $\mathbf{u}(1) \in E^s(p_3)$ are allowed to vary, enables us to find such zeros and, hence, a first connecting orbit comprising the concatenation between $\mathbf{w}$ and $\mathbf{u}$. The concatenated orbit is then followed to sweep out the surface $\mathscr{H}$ by changing the location of the point p_3 on C^3, which is achieved by continuation in B of the coordinate $\mathbf{u}(1)_B$ of $\mathbf{u}(1)$; see [22] for details and more figures.

The orbits used for this sweep can be extended by moving the begin point past the point H. In this way, we are able to visualize how $\mathscr{H}$ transitions through the region with the tourbillon mechanisms, as in Figures 2(b) and 3. Finally, while extending any orbit on $\mathscr{H}$, we can detect when its begin point crosses a chosen section, which may happen only once, as is the case for Λ_{H_B}, or many times, as is the case for $\mathscr{T}$. By requiring the begin point to remain in the chosen section, we are able to compute curves in the intersection set $\mathscr{H} \cap \Lambda_{H_B}$ and $\mathscr{H} \cap \mathscr{T}$, respectively, as in Figures 5, 8 and 9.

Acknowledgments

This research was supported by Royal Society Te Apārangi Marsden Fund grant #16-UOA-286.

References

[1] E. Benoît, J. F. Callot, F. Diener, and M. Diener, *Chasse au canard*, Collectanea Mathematica, 31 (1981), pp. 37–119.

[2] M. Brøns and K. Bar-Eli, *Canard explosion and excitation in a model of the Belousov–Zhabotinskii reaction*, Journal of Physical Chemistry A, 95 (1991), pp. 8706–8713.

[3] M. Brøns, M. Krupa, and M. Wechselberger, *Mixed mode oscillations due to the generalized canard phenomenon*, Fields Institute Communications, (2006), pp. 39–63.

[4] M. Desroches, J. Guckenheimer, B. Krauskopf, C. Kuehn, H. M. Osinga, and M. Wechselberger, *Mixed-mode oscillations with multiple time scales*, SIAM Review, 54 (2012), pp. 211–288.

[5] M. Desroches, B. Krauskopf, and H. M. Osinga, *The geometry of slow manifolds near a folded node*, SIAM Journal on Applied Dynamical Systems, 7 (2008), pp. 1131–1162.

[6] ——, *Mixed-mode oscillations and slow manifolds in the self-coupled FitzHugh-Nagumo system*, Chaos, 18 (2008), p. 015107.

[7] ——, *The geometry of mixed-mode oscillations in the Olsen model for peroxidase-oxidase reaction.*, Discrete & Continuous Dynamical Systems — Series S, 2 (2009), pp. 807–827.

[8] S. Farjami, V. Kirk, and H. M. Osinga, *Computing the stable manifold of a saddle slow manifold.*, SIAM Journal on Applied Dynamical Systems, 17 (2018), pp. 350–379.

[9] N. Fenichel, *Geometric singular perturbation theory for ordinary differential equations*, Journal of Differential Equations, 31 (1979), pp. 53–98.

[10] R. FitzHugh, *Mathematical models of threshold phenomena in the nerve membrane*, The Bulletin of Mathematical Biophysics, 17 (1955), pp. 257–278.

[11] J. Guckenheimer and C. Scheper, *A geometric model for mixed-mode oscillations in a chemical system*, SIAM Journal on Applied Dynamical Systems, 10 (2011), pp. 92–128.

[12] C. Hasan, B. Krauskopf, and H. M. Osinga, *Mixed-mode oscillations and twin canard orbits in an autocatalytic chemical reaction*, SIAM Journal on Applied Dynamical Systems, 16 (2017), p. 21652195.

[13] ——, *Saddle slow manifolds and canard orbits in $\mathbb{R}^4$ and application to the full Hodgkin–Huxley model*, Journal of Mathematical Neuroscience, 8 (2018), p. 5.

[14] A. L. Hodgkin and A. F. Huxley, *A quantitative description of membrane current and its application to conduction and excitation in nerve*, Journal of Physiology, 117 (1952), pp. 500–544.

[15] A. Huber and P. Szmolyan, *Geometric singular perturbation analysis of the Yamada model*, SIAM Journal on Applied Dynamical Systems, 4 (2005), pp. 607–648.

[16] J. L. Hudson, M. Hart, and D. Marinko, *An experimental study of multiple peak periodic and nonperiodic oscillations in the Belousov–Zhabotinskii reaction*, The Journal of Chemical Physics, 71 (1979), pp. 1601–1606.

[17] C. K. R. T. Jones, *Geometric Singular Perturbation Theory*, vol. 1609 of Lecture Notes in Mathematics, Springer-Verlag, New York, 1995.

[18] B. Krauskopf and T. Riess, *A Lin's method approach to finding and continuing heteroclinic connections involving periodic orbits*, Nonlinearity, 21 (2008), pp. 1655–1690.

[19] B. Krauskopf, K. Schneider, J. Sieber, S. Wieczorek, and M. Wolfrum, *Excitability and self-pulsations near homoclinic bifurcations in semiconductor laser systems*, Optics Communications, 215 (2003), pp. 367–379.

[20] C. Kuehn and P. Szmolyan, *Multiscale geometry of the Olsen model and non-classical relaxation oscillations.*, Journal of Nonlinear Science, 25 (2015), pp. 583–629.

[21] A. Milik, P. Szmolyan, H. Löffelmann, and E. Gröller, *Geometry of mixed-mode oscillations in the 3–D autocatalator*, International Journal of Bifurcation and Chaos, 8 (1998), pp. 505–519.

[22] E. Musoke, B. Krauskopf, and H. M. Osinga, *A surface of heteroclinic connections between two saddle slow manifolds in the Olsen model*, International Journal of Bifurcation and Chaos, 30 (2020), p. 2030048.

[23] J. S. Nagumo and S. Arimoto, *An active pulse transmission line simulating nerve axon*, Proceedings of IRE, 50 (1962), pp. 2061–2070.

[24] L. F. Olsen, *An enzyme reaction with a strange attractor*, Physics Letters A, 94 (1983), pp. 454–457.

[25] L. F. Olsen and H. Degn, *Chaos in an enzyme reaction*, Nature, 267 (1977), pp. 177–178.

[26] J. Palis and W. de Melo, *Geometric Theory of Dynamical Systems*, Springer-Verlag, NY, 1982.

[27] L. Perko, *Differential Equations and Dynamical Systems*, Springer International Publishing, 2001.

[28] P. Szmolyan and M. Wechselberger, *Canards in* $\mathbb{R}^3$, Journal of Differential Equations, 177 (2001), pp. 419–453.

[29] K. Tsaneva-Atanasova, H. M. Osinga, T. Riess, and A. Sherman, *Full system bifurcation analysis of endocrine bursting models*, Journal of Theoretical Biology, 264 (2010), pp. 1133 – 1146.

[30] B. Van der Pol, *On "relaxation oscillations"*, The London, Edinburgh, and Dublin Philosophical Magazine and Journal of Science Series 7, 2 (1926), pp. 978–992.

[31] M. Wechselberger, *Existence and bifurcation of canards in* $\mathbb{R}^3$ *in the case of a folded node*, SIAM Journal on Applied Dynamical Systems, 4 (2005), pp. 101–139.